Biochemical Journal (2016) **473** 3205–3219
DOI: 10.1042/BCJ20160294

Research Article

Intermolecular disulfide bond influences unphosphorylated STAT3 dimerization and function

Elena Butturini[1], Giovanni Gotte[1], Daniele Dell'Orco[1], Giulia Chiavegato[1], Valerio Marino[1], Diana Canetti[2,3], Flora Cozzolino[2], Maria Monti[2], Piero Pucci[2] and Sofia Mariotto[1]

[1]Department of Neuroscience, Biomedicine and Movement, Biochemistry Section, University of Verona, Verona, Italy; [2]CEINGE Biotecnologie Avanzate and Department of Chemical Science, University of Naples 'Federico II', Naples, Italy; and [3]Istituto Nazionale di Biostrutture e Biosistemi (INBB), Rome, Italy

Correspondence: Sofia Mariotto (sofia.mariotto@univr.it)

Signal transducer and activator of transcription 3 (STAT3) is a transcription factor activated by the phosphorylation of tyrosine 705 in response to many cytokines and growth factors. Recently, the roles for unphosphorylated STAT3 (U-STAT3) have been described in response to cytokine stimulation, in cancers, and in the maintenance of heterochromatin stability. It has been reported that U-STAT3 dimerizes, shuttles between the cytoplasm and nucleus, and binds to DNA, thereby driving genes transcription. Although many reports describe the active role of U-STAT3 in oncogenesis in addition to phosphorylated STAT3, the U-STAT3 functional pathway remains elusive.

In this report, we describe the molecular mechanism of U-STAT3 dimerization, and we identify the presence of two intermolecular disulfide bridges between Cys367 and Cys542 and Cys418 and Cys426, respectively. Recently, we reported that the same cysteines contribute to the redox regulation of STAT3 signaling pathway both *in vitro* and *in vivo*. The presence of these disulfides is here demonstrated to largely contribute to the structure and the stability of U-STAT3 dimer as the dimeric form rapidly dissociates upon reduction in the S–S bonds. In particular, the Cys367–Cys542 disulfide bridge is shown to be critical for U-STAT3 DNA-binding activity. Mutation of the two Cys residues completely abolishes the DNA-binding capability of U-STAT3. Spectroscopic investigations confirm that the noncovalent interactions are sufficient for proper folding and dimer formation, but that the interchain disulfide bonds are crucial to preserve the functional dimer. Finally, we propose a reaction scheme of U-STAT3 dimerization with a first common step followed by stabilization through the formation of interchain disulfide bonds.

Introduction

The signal transducer and activator of transcription 3 (STAT3) is a member of a family of seven closely related proteins that relay signals from activated cytokines and growth factor receptors in the plasma membrane to the nucleus, in which they regulate gene transcription [1–3]. The domain's arrangement is common to all STATs and encompasses six domains: the N-terminal domain (NTD), the coiled-coil domain (CCD), the DNA-binding domain (DBD), the linker domain (LD), the Src homology 2 domain (SH2), and the transcription activation domain (TAD) at the carboxy-terminus (Figure 1) [4,5]. In addition to full-length proteins, several shorter proteins exist, arising from alternative splicing and proteolytic process [6].

According to the canonical pathway, STAT3 is activated in response to a wide range of growth factors and cytokines by phosphorylation at the specific tyrosine residue (Tyr705) located near the carboxy-terminal domain. This activation step requires receptor-associated protein tyrosine kinases of the JAK or Src family. On activation, the phosphorylated STAT3 (pSTAT3) molecules dimerize through the interaction of SH2 domain and translocate from the cytoplasm to the nucleus. The dimer

Received: 5 April 2016
Revised: 15 July 2016
Accepted: 2 August 2016

Accepted Manuscript online: 2 August 2016
Version of Record published: 27 September 2016

PORTLAND PRESS

Biochemical Journal (2016) **473** 3205–3219
DOI: 10.1042/BCJ20160294

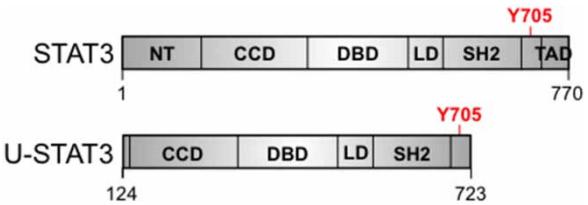

Figure 1. Structure of U-STAT3.

Schematic representation of the six domains of STAT3, NTD, CCD, DBD, LD, an SH2, and TAD. A tail segment containing the phosphorylation site Y705 is located between the SH2 and TAD domains. The construct used (U-STAT3) comprises residues 124–723 and lacks the N-terminal co-operativity domain as well as the C-terminal transactivating domain.

binds to target DNA motifs and promotes the expression of a large variety of genes, encoding mediators crucial for the classic physiological acute phase response or involved in a variety of critical cell functions, including differentiation, proliferation, apoptosis, angiogenesis, metastasis, and immune response [7–9]. Several post-translational modifications, such as S-glutathionylation, methylation, acetylation, and S-nitrosylation, have also been identified for STAT3; some are believed to control dimerization, but others affect the nuclear import/export or DNA binding [10–14]. Although STAT3 activation normally leads to the physiological response, deregulation of this transduction cascade could promote tissue damage and could be directly or indirectly involved in different inflammatory-related diseases [15–19]. Furthermore, accumulating evidence shows that STAT3 is overexpressed and constitutively activated in several human cancers [5,20,21]. The abnormal constitutive activation of STAT3 stimulates its own transcription, causing an increase in unphosphorylated STAT3 (U-STAT3), which drives the expression of a set of genes distinct from those activated by pSTAT3, thus contributing to tumorigenesis [22,23]. Although it was initially reported that U-STAT3 is monomeric in its latent state, several studies indicate the presence of dimeric or higher molecular weight complexes, termed 'statosome', in cell extracts or in *in vitro* studies [24,25]. It has been reported that U-STAT3 dimerizes, shuttles between the cytoplasmic and nuclear compartments, and binds to DNA, but it is not clear how U-STAT3 drives genes transcription. Yang et al. [26] described that U-STAT3 binds to unphosphorylated NFκB (U-NFκB), in competition with IκB, and the resulting U-STAT3/U-NFκB complex accumulates in the nucleus with the help from the nuclear localization signal of STAT3 and activates a subset of NFκB-dependent genes. Previously, using 100-fold molar excess, the U-STAT3 core (lacking the NTD) was shown to bind directly to a GAS consensus sequence and also to AT-rich hairpin and cruciform DNA structure in the monomeric as well as in the dimeric form [27]. Although a number of reports describe the active role of U-STAT3 in oncogenesis in addition to pSTAT3, the U-STAT3 functional pathway still needs to be elucidated. Structural studies on U-STAT3 dimerization are necessary to clarify the conformational changes, regulating its nuclear translocation and DNA binding.

In this report, we describe the molecular mechanism of U-STAT3 dimerization in the recombinant purified form. We identified the presence of two intermolecular disulfide bridges linking Cys367 and Cys542 and Cys418 and Cys426, respectively. Then, we investigated U-STAT3 stability using biophysical approaches showing that dimerization of U-STAT3 is crucial for DNA-binding activity. Two double mutants, constructed by changing either Cys pair into Ser residues, demonstrated that the absence of the Cys367–Cys542 disulfide completely abolishes U-STAT3 DNA-binding ability. Finally, on the basis of our results, we propose a multistate equilibrium process for U-STAT3 dimerization.

Experimental procedures

Reagents

All chemicals used throughout the present study were of the highest analytical grade, purchased from Sigma (Milan, IT), unless otherwise specified.

Expression and purification of wild-type and mutant U-STAT3

The full-length cDNA coding for human STAT3 (STAT3α) cloned on a pOTB-STAT3 vector was purchased from ImaGENES. STAT3α expression construct coding for aminoacid residues 124–723 (U-STAT3; Figure 1) was amplified by polymerase chain reaction and cloned into the *Sal* I-*Not* I site of the expression vector

Biochemical Journal (2016) **473** 3205–3219
DOI: 10.1042/BCJ20160294

pGEX4T1 (GE Healthcare), and C367/542S and C418/426S U-STAT3 mutants were generated by QuikChange site-directed mutagenesis kit (Stratagene) and cloned into the *Sal* I-*Not* I site of the expression vector pGEX4T1. The U-STAT3 plasmids obtained were transformed into the *Escherichia coli* strain BL21 (DE3, New England BioLab, Inc.). Recombinant clones were analyzed by DNA sequence. The recombinant proteins were purified by Glutathione Chromatrix™ (Jena Bioscience) and eluted in 20 mM Tris–HCl, pH 8.5, and 150 mM NaCl [11].

Size-exclusion chromatography

The analysis of the aggregation profiles of U-STAT3 was performed with a Superdex 200 HR 10/300 column (GE-Healthcare), connected to a ÄKTA-FLPC purifier system (GE-Healthcare) and equilibrated with 20 mM Tris–HCl, pH 5.0, or 8.5/150 mM NaCl buffer. The column was calibrated with six molecular mass standards (ferritin 420 kDa; aldolase 158 kDa; bovine serum albumin 66 kDa; lactoalbumin 45 kDa; carbonic anydrase 29 kDa; and RNAsi 13.7 kDa).

Approximately 100–500 μL of U-STAT3 (0.5–1 mg/ml) were incubated under different experimental conditions and centrifuged (20 000 × ***g***, 4°C, 10 min) to discard large aggregates. The supernatant was then injected onto the column and eluted at a flow rate of 0.12–0.15 ml/min. The analysis of the patterns obtained and measurement of the areas of the peaks were performed with the Unicorn 5.01 Software (GE Healthcare).

STAT3/JAK2 kinase assay

STAT3/JAK2 (Janus kinase 2) kinase assay was performed using recombinant JAK2 active protein (Upstate Biotechnology), as described elsewhere [11,28,29], with slight modification. Briefly, kinase reactions were performed by incubating 1 μg of U-STAT3 with 10 ng of JAK2 protein in 30 μl of kinase reaction buffer (20 mM Tris–HCl, pH 7.5, 50 mM $MgCl_2$, and 100 μM ATP). Samples were incubated at 20°C for 10 min within the linear reaction range, and reactions were stopped by the addition of reducing SDS sample buffer. Samples were then boiled, separated by SDS–PAGE, and immunoblotted with anti-pTyr^{705} STAT3 antibody (Cell Signaling Technology). To verify the autophosphorylation of JAK2, membranes were rehybridized with anti-pTyr$^{1007/1008}$ JAK2 antibody (Millipore). After being stripped, the membranes were rehybridized with anti-STAT3 K-15 antibody (Santa Cruz Biotechnology) and anti-JAK2 antibody (Cell Signaling Technology).

Electrophoretic mobility shift assay

The DNA-binding activity of U-STAT3 was assayed with a ^{32}P-labeled M67 probe (5′-gtcgaCATTTCCC GTAAATCg-3′). The probe was prepared by the end-labeling of double-stranded oligonucleotides with [^{32}P]ATP and T4-polynucleotide kinase. U-STAT3 (0.1 μM) was incubated with 2–5 × 10^4 cpm of ^{32}P-labeled double-stranded oligonucleotides in binding buffer containing 20 mM HEPES, pH 7.9, 50 mM KCl, 0.1 mM EDTA, 2 μg of poly(dI-dC), and 1 μg of salmon sperm DNA. Products were fractionated on a nondenaturing 5% polyacrylamide gel. Gels were dried and auto-radiographed, and the intensity of hybridization was quantified using the public domain NIH Image 1.61 program (developed at the U.S. National Institutes of Health and available on http://rsb.info.nih.gov/nih-image/). To control the DNA-binding specificity, a scrambled M67 sequence was used.

Mass spectrometry analysis

The protein band, showing the electrophoretic mobility compatible with U-STAT3 dimer on a nonreducing gel, was excised from the gel, destained by washing with acetonitrile and 50 mM ammonium bicarbonate, and hydrolyzed with 20 ng of trypsin in 50 mM ammonium bicarbonate, pH 8.0, at 37°C overnight. The peptide mixture was extracted from the gel by acetonitrile and 0.2% formic acid washing and dried in a speed vac system. It was then directly analyzed by MALDI-MS onto a 4800 plus MALDI TOF–TOF mass spectrometer (ABI SCIEX) equipped with a reflectron analyzer and used in delayed extraction mode with 4000 Series Explorer, v3.5 Software. An aliquot of the same peptide mixture was treated with 50 mM DTT in 50 mM ammonium bicarbonate, pH 8.0, at 37°C for 1 h, to reduce disulfide bonds. The peptide mixture was then acidified and directly analyzed by MALDI-MS.

For MALDI analysis, 0.5 μl of each peptide mixture was mixed with an equal volume of α-cyano-4-hydroxycinnamic acid as matrix (10 mg/ml in 0.2% TFA in 70% acetonitrile), loaded onto the metallic sample plate, and air-dried. Mass calibration was performed with the standard mixture provided by the manufacturer. MALDI-MS data were acquired over a 600−6000m/z mass range in the positive ion reflector mode.

Biochemical Journal (2016) 473 3205–3219
DOI: 10.1042/BCJ20160294

Dynamic light scattering

Dynamic light scattering (DLS) measurements were performed on the samples of monomeric U-STAT3 as described recently [30] in 20 mM Tris–HCl, pH 8.5, 150 mM NaCl frozen immediately after their purification with size-exclusion chromatography (SEC). In brief, a Zetasizer Nano-S (Malvern Instruments) and polystyrene low volume disposable sizing cuvettes (ZEN0112) were used for the experiments. Viscosity and refractive index were set at 0.8872 cP and 1.330 (default values for water), respectively; temperature was set to 10°C, with 10 min equilibration time. The measurement angle was 173° backscatter, and the analysis model was set to multiple narrow modes. For each measurement, a minimum of 30 determinations were performed, each consisting of 12–16 repetitions. The same sample was stored at 10°C between subsequent measurements. Each recording lasted ∼2 h, and experiments were run for 4 days in the morning and in the afternoon, with an interval of ∼4 h between subsequent experiments run on the same day.

Circular dichroism spectroscopy and thermal denaturation studies

Circular dichroism (CD) spectroscopy studies were performed essentially as described recently for U-STAT3 [11]. A Jasco V-710 spectropolarimeter equipped with a Peltier-type thermostated cell holder was used to record both near-UV (250–320 nm; 1-cm cuvette) and far-UV spectra (200–250 nm; 0.1 cm cuvette) of monomeric and dimeric U-STAT3, right after separation by SEC. Spectra were recorded at 25°C at a scan rate of 50 nm/min, bandwidth of 1 nm, and integration time of 4 s. Five spectra accumulations were averaged for each sample.

Thermal denaturation of both monomeric and dimeric U-STAT3 was monitored between 10 and 96°C, using the same conditions as for the far-UV spectra. The ellipticity signal at 208 nm (θ_{208}) was recorded at a scan rate of 1°C/min and at a response time of 4 s, using a 0.1 cm quartz cuvette.

The analysis of thermal denaturation curves was performed for each sample, assuming a two-state transition process. Complete unfolding was achieved for both monomeric and dimeric U-STAT3 under the experimental conditions used, as shown by the residual CD signal resulting after thermal denaturation (results not shown). Data were fitted according to a four-parameter Hill sigmoid:

$$y = b_{\mathrm{n}} + \frac{|b_{\mathrm{n}} - b_{\mathrm{u}}|T^{H}}{T_{\mathrm{m}}^{H} + T^{H}}$$

where b_{n} is the baseline value (θ_{208}) of the native protein, b_{u} is the baseline value of the unfolded protein, T is the temperature, H is the Hill coefficient, and T_{m} is the melting temperature.

Surface plasmon resonance

The kinetics of U-STAT3 dimerization was examined by surface plasmon resonance (SPR), using SensQ Pioneer biosensor system at a controlled temperature of 15°C. The SEC-purified U-STAT3 monomer ('ligand STAT3', $^{\mathrm{L}}$STAT3) was dissolved in sodium acetate buffer, pH 5.0, and immobilized onto COOH5 sensor chip (Sens.Q Technologies), by standard amine-coupling reaction up to responses of 5000 resonance units (RU). A reference flow cell was prepared by the same procedure in the absence of protein. Increasing concentrations (0.05×10^{-6} up to 2.5×10^{-6} M) of recombinant U-STAT3 ('analyte STAT3', $^{\mathrm{A}}$STAT3) were injected at a flow rate of 10 μl/min for 30 min in running buffer (20 mM Tris, pH 8.5, 150 mM NaCl), and the dissociation of bound proteins was monitored for 60 min. For all analyses, reference flow cell sensorgrams were subtracted from ligand flow cell sensorgrams.

The association and dissociation rate constants k_{a} and k_{d}, respectively, for the $^{\mathrm{L}}$STAT3–$^{\mathrm{A}}$STAT3 complexes, were determined by direct curve fitting of the sensorgrams, assuming a 1:1 Langmuir model according to eqns 1 and 2, relative to the association and dissociation phases, respectively:

$$\mathrm{RU} = \mathrm{RU}t_0 + (k_{\mathrm{a}}[\mathrm{C}]\mathrm{RUmax})(1 - e^{-(k_{\mathrm{a}}[\mathrm{C}]+k_{\mathrm{d}})t})/(k_{\mathrm{a}}[\mathrm{C}] + k_{\mathrm{d}}) \quad (1)$$

$$\mathrm{RU} = -k_{\mathrm{d}}\mathrm{RU}t_0 * e^{-k_{\mathrm{d}}(t-t_0)} \quad (2)$$

where RU is the signal response; RUmax, the maximum response level; RUt_0, the response at the beginning of the dissociation phase; and [C], the molar concentration of $^{\mathrm{A}}$STAT3. The dissociation equilibrium constant,

Biochemical Journal (2016) **473** 3205–3219
DOI: 10.1042/BCJ20160294

K_D, was calculated as k_d/k_a. The dissociation phase was analyzed first, and the obtained k_d value (eqn 2) was kept constant and used in eqn 1.

Kaleidagraph software (version 6.0; GraphPad Software, Inc.) was used for the analysis of SPR data.

Results

STAT3 dimerizes in the absence of tyrosine phosphorylation

To evaluate the dimerization and aggregation propensity of recombinant U-STAT3, we performed SEC following protein incubation under different experimental conditions, including temperature, protein concentration, time, and pH.

The protein extensively aggregates at temperatures exceeding 10°C, thus several attempts were performed to settle the right compromise to obtain a large enough amount of dimer and to avoid extensive U-STAT3 aggregation. We evaluated the effect of U-STAT3 dimerization tendency at 10°C in 20 mM Tris–HCl, pH 8.5, 150 mM NaCl until 5-day incubation time. As shown in Figure 2A, U-STAT3 (1 mg/ml) eluted at t_0 as a major peak at ∼15.4 ± 0.1 ml corresponding to a monomer with an apparent MW of ∼80 kDa (solid line) preceded by a small shoulder. The major peak (M) and the preceding shoulder (D) were analyzed by nonreducing SDS–PAGE and immunoblotted using anti-STAT3 antibody (Figure 2A, insert). After 24 h incubation, the shoulder increased and eluted at ∼14.3 ± 0.1 ml, corresponding to a MW approximately twice that of the monomer. The shoulder D progressively increased if the incubation time is extended to 3 days, and after 5 days also larger aggregates were detected, together with species not retained by the column (Figure 2A). Following several attempts, the best compromise to obtain a certain amount of dimeric U-STAT3, but avoiding extensive aggregation, was established, protein concentration 1 mg/ml, temperature 10°C, and 3-day incubation time.

To clarify the molecular mechanism of U-STAT3 dimerization, we studied the monomer/dimer equilibrium at different pH values, which probably regulate the reactivity of cysteine residues and might affect the intermolecular disulfide formation. U-STAT3 was incubated under the previously defined conditions in 20 mM sodium acetate buffer, pH 5.5, containing 150 mM NaCl. As shown in Figure 2B, U-STAT3 eluted as a single peak at 15.5 ± 0.1 ml at pH 5.5, indicating that the protein is almost totally present in the monomeric form, while at pH 8.5 a consistent amount of dimeric form was present. The pH dependence of the monomer/dimer equilibrium suggests that intermolecular disulfide bridges might promote and stabilize the dimer formation.

Time course of U-STAT3 dimerization monitored by DLS

The results obtained with SEC (Figure 2A) suggested that dimerization of U-STAT3 might be a dynamic process involving specific time frames. To explore this possibility, we performed DLS experiments by monitoring the size of U-STAT3 species on a regular basis over a 3-day time frame, at 10°C (Supplementary Figure S1). The suspension showed satisfactory colloidal properties and appeared to be substantially monodisperse during the first 2 h (Supplementary Figure 1SA), with a high intensity peak corresponding to a hydrodynamic diameter $d_1 = 12.4 \pm 0.4$ nm, involving ∼87% of the scattered light intensity and fairly low polydispersity index (pdI = 0.24). Already in the following 2 h, the average size of the suspension increased, and a population with higher hydrodynamic diameter appeared (Supplementary Figure S1B). Interestingly, both the size of the most intense peak ($d_1 = 16.0 \pm 0.9$ nm) and the polydispersity index (pdI = 0.42) increased. The same trend was observed after overnight incubation (Supplementary Figure S1C; $d_1 = 18.2 \pm 1.1$ nm; pdI = 0.41). However, starting from the second day, the size distribution appeared generally broader (Supplementary Figure S1D) with the onset of intermediate size peaks, that is, 20–100 nm (as shown in the plot of the mean size distribution overlapped to individual recordings in Supplementary Figure S1K). The size distribution did not significantly change after a second and a third overnight incubation steps (Supplementary Figure S1E–G). The addition of 15 μM DTT, that is, in slight excess to U-STAT3 concentration (∼10 μM), did not significantly modify the size distribution (Supplementary Figure S1H). To estimate the size of the most intense peaks, the sample underwent a mild centrifugation step (20 000 × ***g***, 4°C, 15 min), resulting in a predominant peak (Supplementary Figure S1I) corresponding to a hydrodynamic diameter $d_1 = 18.2 \pm 1.2$ nm, with an intensity of 77.4% and fairly low pdI (0.26). Interestingly, further addition of DTT to a final concentration of 2 mM, without any further centrifugation, significantly decreased the size of the predominant peak ($d_1 = 13.9 \pm 1.5$ nm), bringing it back to values essentially comparable to the initial monomeric conditions (Supplementary Figure S1A,K).

Biochemical Journal (2016) **473** 3205–3219
DOI: 10.1042/BCJ20160294

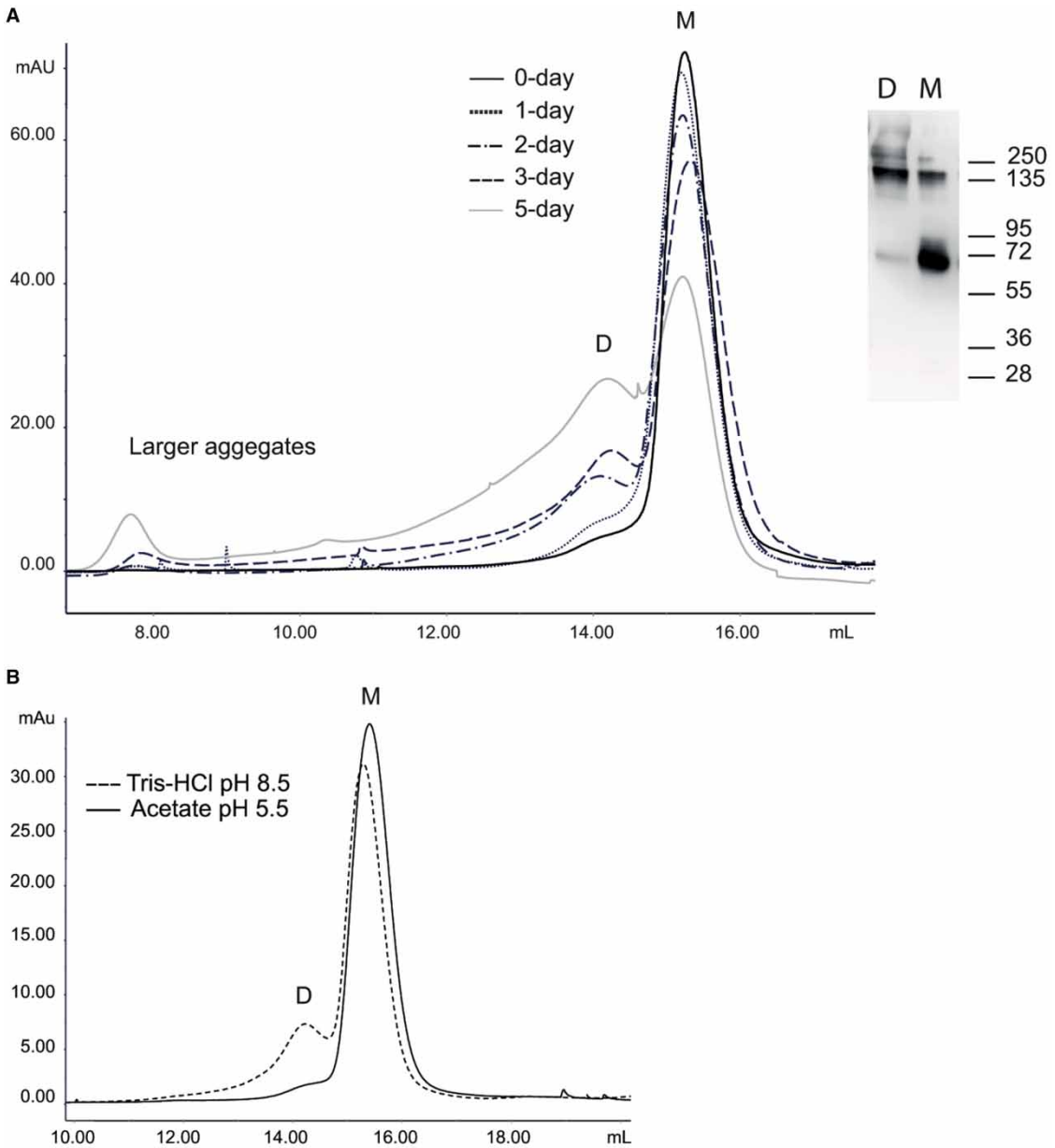

Figure 2. SEC analysis of U-STAT3 self-association.

(**A**) Time-dependence of U-STAT3 self-association. Protein (1 mg/ml) was incubated at 10°C in 20 mM Tris–HCl buffer, pH 8.5, containing 150 mM NaCl. Aliquots of 200 μl were withdrawn at times indicated in the panel, centrifuged, and supernatants were injected onto a Superdex 200 HR 10/300 column equilibrated with the same buffer. Insert: nonreducing SDS–PAGE and western blot with anti-STAT3 antibody analyses of monomer (M) and dimer (D) U-STAT3. Bands at ~67 and 130 kDa were revealed and assigned to U-STAT3 monomer and dimer species, respectively. (**B**) pH-dependence of U-STAT3 self-association. Protein (1 mg/ml) was incubated at 10°C either in 20 mM sodium acetate (pH 5.5, solid line) or in 20 mM Tris–HCl buffer (pH 8.5, dashed line), both containing 150 mM NaCl. Following 3-day incubation, samples were centrifuged, and 200 μl of the supernatant were injected onto a Superdex 200 HR 10/300 column.

The results of DLS experiments are consistent with a dynamically slow formation of STAT3 oligomers under the conditions tested. Moreover, the clearly visible effect of DTT on the size distribution of U-STAT3 species strongly suggests the involvement of disulfide bridges in the dimerization/oligomerization process.

Biochemical Journal (2016) **473** 3205–3219
DOI: 10.1042/BCJ20160294

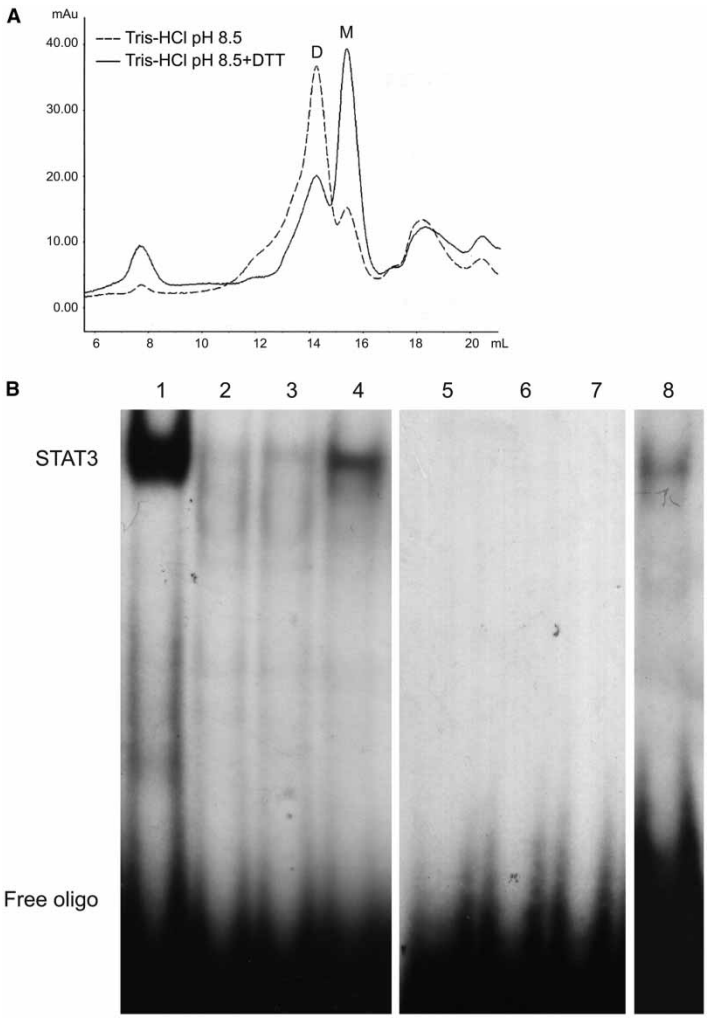

Figure 3. Redox stability and functional analysis of U-STAT3 dimer.

(**A**) Effect of DTT on dimeric U-STAT3. The dimeric U-STAT3 fraction eluted from SEC was collected and divided into two aliquots. The first one was immediately reinjected onto the Superdex 200 HR 10/300 column (dashed line), while the other was incubated with DTT for 4 h and then was injected in the same column (solid line). (**B**) DNA-binding activity of U-STAT3. U-STAT3 dimer (lane 1), U-STAT3 monomer (lane 2), C367/542S mutant (lane 3), and C418/426S mutant (lane 4) were incubated with M67 dsDNA and analyzed by EMSA. U-STAT3 dimer was also incubated with M67 dsDNA in the presence of 10 μM DTT (lane 8). As a negative control, U-STAT3 dimer (lane 5), C367/542S mutant (lane 6), and C418/426S mutant (lane 7) were incubated with M67 scramble dsDNA. The image is representative of four independent experiments.

Interchain disulfide bonds are involved in STAT3 dimer stabilization

To better characterize the U-STAT3 dimerization, the dimeric fraction eluted from SEC was collected and divided into two aliquots. The first one was immediately incubated for 4 h in ice with DTT in a 1/1.2 protein/reducing agent molar ratio and then reexamined by SEC. The second aliquot was directly reinjected onto the column (Figure 3A, dashed line). In the presence of DTT, U-STAT3 eluted as a highly predominant peak at a volume corresponding to the MW of the monomeric form with a minor residual of dimeric peak (Figure 3A, solid line). The untreated portion of the dimeric U-STAT3 fraction exhibited the expected elution volume corresponding to the protein dimeric form. These data further provide strong evidence for the presence of interchain disulfide bonds in the U-STAT3 dimeric form.

Previously, the U-STAT3 core had been shown to bind directly to a GAS or cfos consensus sequence [27,31]. Hence, the DNA-binding activity of both monomeric and dimeric U-STAT3 was evaluated here by

Biochemical Journal (2016) **473** 3205–3219
DOI: 10.1042/BCJ20160294

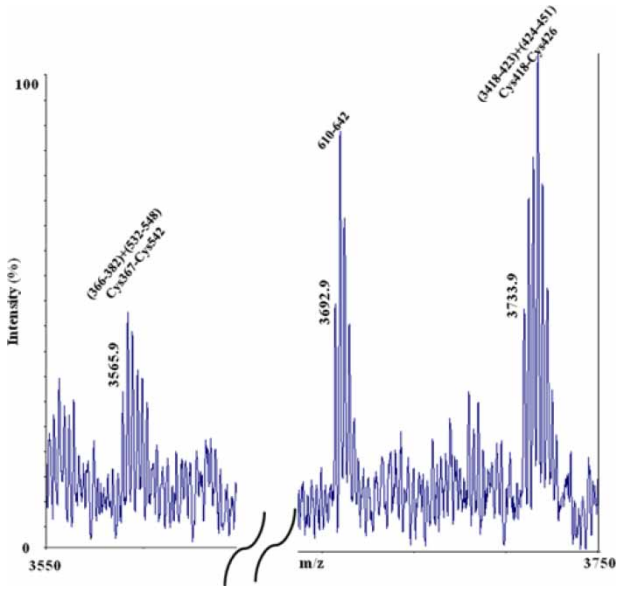

Figure 4. Partial MALDI-MS spectra of the tryptic digest from STAT3 dimeric form.

The dimeric U-STAT3 fraction eluted from SEC was digested with trypsin, and the resulting peptide mixture was directly analyzed by MALDI-MS. The mass signals at 3565.9 and 3733.9 were associated to the peptides pairs 366–382 and 532–548 and 418–423 and 424–451, respectively, jointed by the disulfide bridges Cys367–Cys542 and Cys418–Cys426, respectively.

electrophoretic mobility shift assay (EMSA) analysis using M67 dsDNA that is a modified cfos-inducible enhancer. Figure 3B reveals that dimeric U-STAT3 was able to bind DNA (Figure 3B, lane 1), whereas monomeric U-STAT3 did not show any DNA-binding capability (Figure 3B, lane 2). The addition of 1 mM DTT to the binding buffer noticeably decreased the DNA-binding activity of dimeric U-STAT3, thus demonstrating the contribution of interchain disulfide bonds in U-STAT3 functional activity (Figure 3B, lane 8).

Interchain disulfide bonds assignment

The identification of cysteine pairings in U-STAT3 dimer was carried out using the MALDI mapping strategy [11]. The dimeric fraction of recombinant U-STAT3 protein purified by SEC was loaded onto a nonreducing polyacrylamide gel to further purify the dimer from monomer contamination. The protein band, showing the electrophoretic mobility expected for U-STAT3 dimer, was excised from the gel and digested with trypsin. The resulting peptide mixture was extracted from the gel and directly analyzed by MALDI-MS. Most of the signals recorded in the mass spectra were mapped onto the anticipated U-STAT3 sequence. However, two signals occurring at *m*/*z* 3565.9 and 3733.9, respectively (Figure 4), could not be assigned to any peptide present in the protein sequence and were then tentatively considered as putative S–S-containing fragments. The signal at *m*/*z* 3565.8 was interpreted as arising from peptides (366–382) and (532–548) linked by a disulfide bond between Cys367 and Cys542. Analogously, the MH^+ signal at *m*/*z* 3733.9 was assigned to a two-peptide cluster involving fragments (418–423) and (424–451) linked by the disulfide bond between Cys418 and Cys426. Table 1 reports the results of the MALDI analysis of the peptides containing disulfide bond(s).

These findings were confirmed after reexamining by MALDI-MS the peptide mixture resulting after reduction with DTT, which showed the disappearance of the S–S bridges containing signals (data not shown).

Dimerization of U-STAT3 mutants

The role played by the identified cysteines in U-STAT3 dimerization and the DNA-binding activity was evaluated by generating two double mutants in which both the two cysteine pairs involved in S–S bonds were substituted with serine. As demonstrated by *in vitro* tyrosine kinase assay, the tyrosine phosphorylation site was not affected in the two mutants, thus indicating that the mutations did not alter the gross conformation of the protein (Supplementary Figure S2). As expected, SEC analyses clearly indicated that both U-STAT3 mutants were present in the dimeric form, due to the presence of the remaining S–S bridge (Figure 5A,B, solid line). In

Biochemical Journal (2016) **473** 3205–3219
DOI: 10.1042/BCJ20160294

Table 1 MALDI-MS analysis of disulfide bridges containing peptides from the tryptic digest of dimeric U-STAT3

The theoretical MH^+ values of reduced peptides are also indicated.

Observed MH^+	Theoretical MH^+ of reduced peptides	Peptides	S–S
3565.8	1761.9, 1806.9	(366–382) + (532–548)	C367–C542
3733.9	563.2, 3173.6	(418–423) + (424–451)	C418–C426

the presence of DTT, in fact, both mutants eluted as a highly predominant peak associable to a MW corresponding to the monomeric form (Figure 5A,B, dot line). However, subtle differences could be detected in the two mutants. The mutant lacking the Cys367–Cys542 disulfide bond produced a major unresolved peak (Figure 5A), whereas the absence of the Cys418–Cys426 bridge gave rise to an elution profile similar to the one shown by wild–type (WT) U-STAT3, although with a definitely minor amount of dimeric form. On the basis of these results, we speculate that the lack of Cys367–Cys542 intermolecular disulfide should trigger structural changes that alter the overall conformation of the dimeric species.

The DNA-binding capability of U-STAT3 mutants was investigated by EMSA analyses. According to our hypothesis, only the DNA-binding capability of U-STAT3 lacking the Cys367–Cys542 disulfide was completely abrogated (Figure 3B, lane 3), suggesting an essential role of this disulfide bridge in conferring to dimeric U-STAT3 the proper conformation to bind DNA.

On the other hand, U-STAT3 lacking the Cys418–Cys426 disulfide bridge still retains a little DNA-binding ability due to the presence of small amount of U-STAT3 dimer (Figure 3B, lane 4), again underlining the importance of Cys367–Cys542 S–S for the stability of a functional dimer.

STAT3 monomer and dimer have similar secondary and tertiary structure and thermal stability

To check for structural differences between monomeric and dimeric U-STAT3 forms, the fractions collected from SEC were analyzed by CD spectroscopy. As shown in Supplementary Figure S3, no substantial differences could be observed in the spectra both in the far- (200–250 nm) and in the near-UV (250–320) range, indicating that dimeric U-STAT3 preserves monomer-like secondary and tertiary structures under the tested conditions.

To investigate the thermal stability of both monomeric and dimeric U-STAT3 species, we took advantage of the high α-helix content of the protein, which is reflected by the typical minima in the far-UV CD spectra at 208 and 222 nm (Supplementary Figure S3). The ellipticity at 208 nm (θ_{208}) was monitored also at increasing the temperature from 10 to 96°C (Figure 6). Monomeric and dimeric U-STAT3 showed very similar thermal denaturation profiles. Both forms exhibited a sigmoidal trend compatible with a two-state unfolding process, with very similar melting temperatures (T_m^{mon} = 57.9°C and T_m^{dim} = 59.1°C) and very high Hill coefficients (26.5 for the monomer and 36.9 for the dimer), indicative of a highly cooperative transition process occurring without the involvement of partly folded intermediates. This finding, together with the very similar spectroscopic features observed for the monomeric and dimeric forms of U-STAT3 (Supplementary Figure S3), suggests that the thermal unfolding of the monomers within the covalently bound dimer essentially occurs independently of one another.

Association/dissociation kinetics of U-STAT3 monomers investigated by surface plasmon resonance

To characterize the specific binding event occurring between U-STAT3 monomers, SPR was performed on 20 different injections, assuming a simple dimerization scheme in which homodimerization was modeled as a pseudo-first-order process, while the dissociation reaction as a first-order process. The SEC-purified U-STAT3 monomer (ligand STAT3, ^{L}STAT3) was immobilized on a sensor chip at 5000 RU (corresponding to ∼8 ng of protein), and the SEC-purified U-STAT3 monomer (analyte STAT3, ^{A}STAT3) was used as the analyte. The concentration of ^{A}STAT3 ranged between 0.05 and 3 μM. Interestingly, within a broad range of ^{A}STAT3 concentrations (0.05 μM up to 0.25 μM), the proposed kinetic model nicely fitted the experimental data (Figure 7), leading to relatively low rate constants for both association ($k_a = 4.19 \times 10^4 \pm 0.98 \times 10^4$ M^{-1} s^{-1}) and dissociation kinetics ($k_d = 3.94 \times 10^{-4} \pm 0.13 \times 10^{-4}$ s^{-1}), thus resulting in an average apparent affinity, K_D =

Biochemical Journal (2016) **473** 3205–3219
DOI: 10.1042/BCJ20160294

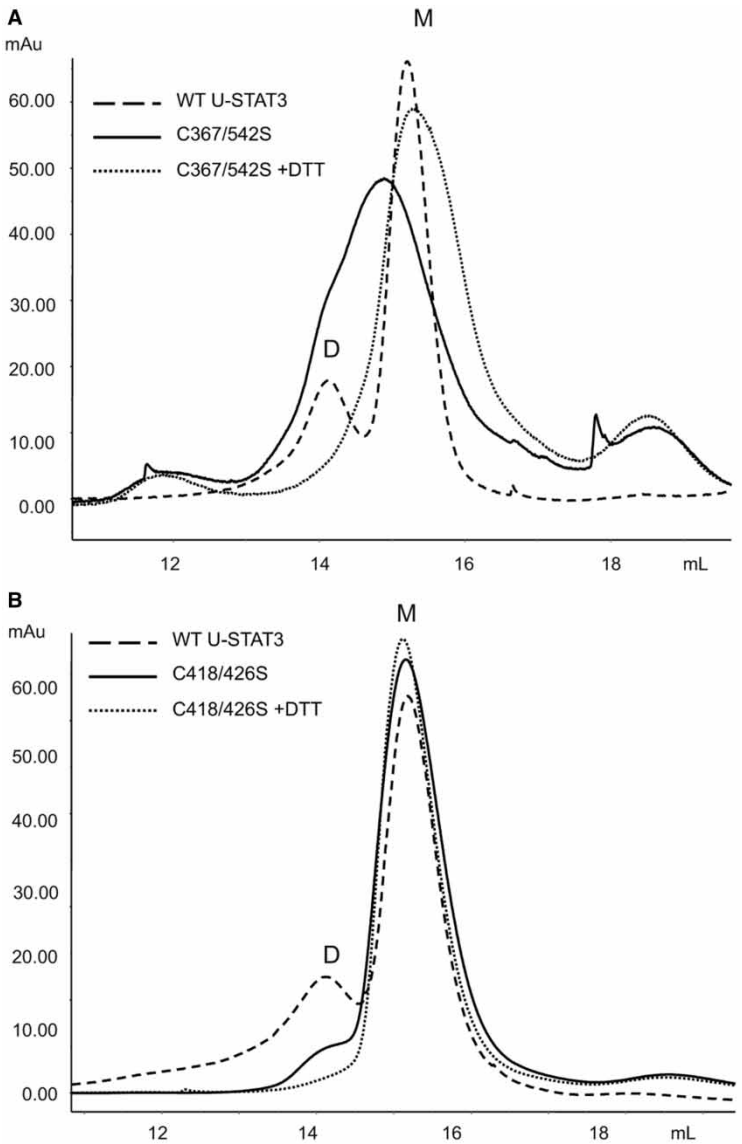

Figure 5. Dimerization of U-STAT3 mutants.

The two U-STAT3 double mutants (1 mg/ml) were incubated at 10°C in 20 mM Tris–HCl buffer, pH 8.5, containing 150 mM NaCl. After 3-day incubation, samples were centrifuged, and 200 μl of the supernatants were injected onto a Superdex 200 HR 10/300 column and compared with WT. For S–S bridges reduction, samples were treated with 2 mM DTT for 4 h and then reinjected onto the column. (**A**) The C367/542S U-STAT3 mutant and (**B**) the C418/426S U-STAT3 mutant.

9.40 nM. However, higher concentrations of ^{A}STAT3, in the range 0.4 −3 μM, resulted in association paths that were incompatible with the proposed mechanism, as neither a clear dependence on the analyte concentration nor saturation after injection could be observed in any case (data not shown).

At the tested SPR experimental conditions, the protein binding detected mimics the dimerization process measured as the ability of ^{A}STAT3 to bind to the immobilized ^{L}STAT3, but it cannot reveal the formation of disulfide bridges, an event whose detection requires conditions and time frames that are unsuitable for on-chip analysis.

Discussion

Recent studies demonstrate that, besides pSTAT3, also U-STAT3 can dimerize, translocate to the nucleus, and bind to the STAT3-binding sites, thereby activating the transcription of target genes. In the present paper, the

Biochemical Journal (2016) **473** 3205–3219
DOI: 10.1042/BCJ20160294

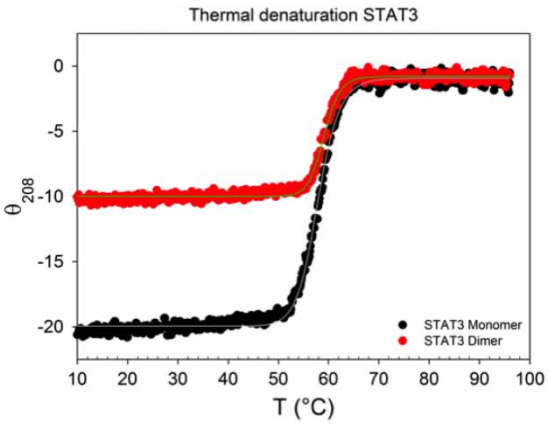

Figure 6. Thermal denaturation of U-STAT3 monitored by CD spectroscopy.

Thermal denaturation of both monomeric and dimeric U-STAT3 in 20 mM Tris–HCl buffer, 150 mM NaCl, pH 8.5, was followed by monitoring the ellipticity signal at 208 nm over a 10–96°C temperature range. Protein concentration was ~1 mg/ml for the monomer and 0.5 mg/ml for the dimer. Quantitative data obtained by fitting the experimental curve to a sigmoidal function led to the following melting temperatures, corresponding to half-maximal denaturation conditions: $T_m^{mon} = 57.9^{\circ}C$ (Hill coefficient, $h = 26.5$) for the monomer and $T_m^{dim} = 59.1°C$ ($h = 36.9$) for the dimer.

biochemical properties of purified recombinant U-STAT3 were investigated to understand the molecular mechanisms underlying U-STAT3 dimerization. The STAT3 core (residues 124–723) lacking the NT-domain was expressed in *E. coli* strain BL21, and the identity of the eluted proteins was confirmed by immunoblot analysis that results in a major protein band of ~67 kDa and by MALDI mapping. The correct folding and biological activity were assessed by CD measurements and protein kinase assay [11]. Nonreducing SDS–PAGE, gel filtration, and DLS experiments suggested the existence of intermolecular disulfide bond linking two U-STAT3 monomers. Mass mapping experiments confirmed these data, indicating the occurrence of two intermolecular S–S bridges joining Cys367–Cys542 and Cys418–Cys426, respectively. The presence of these disulfides was demonstrated to largely contribute to the structure and stability of U-STAT3 dimer, as the dimeric form rapidly dissociates on reduction in the S–S bonds.

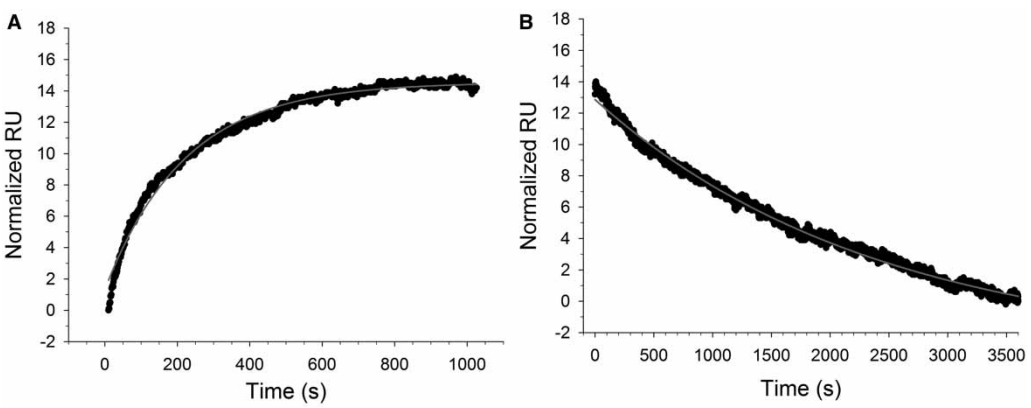

Figure 7. Kinetic analysis of U-STAT3 dimerization.

(**A** and **B**) Reference subtracting association and dissociation sensorgram corresponding to 125 nM of ^{A}U-STAT3. Data were fitted according to a simple concerted model, which separately considers the dissociation (k_d) and the association processes (k_a) (black lines). The obtained kinetic parameters for this example are $k_d = 4.13 \times 10^{-4}$ s^{-1} and $k_a = 3.2 \times 10^{4}$ M^{-1} s^{-1}. Mean and standard deviations for kinetic parameters were assessed from 20 different experiments in which [^{A}U-STAT3] varied from 0.05 to 0.3 μM.

Biochemical Journal (2016) **473** 3205–3219
DOI: 10.1042/BCJ20160294

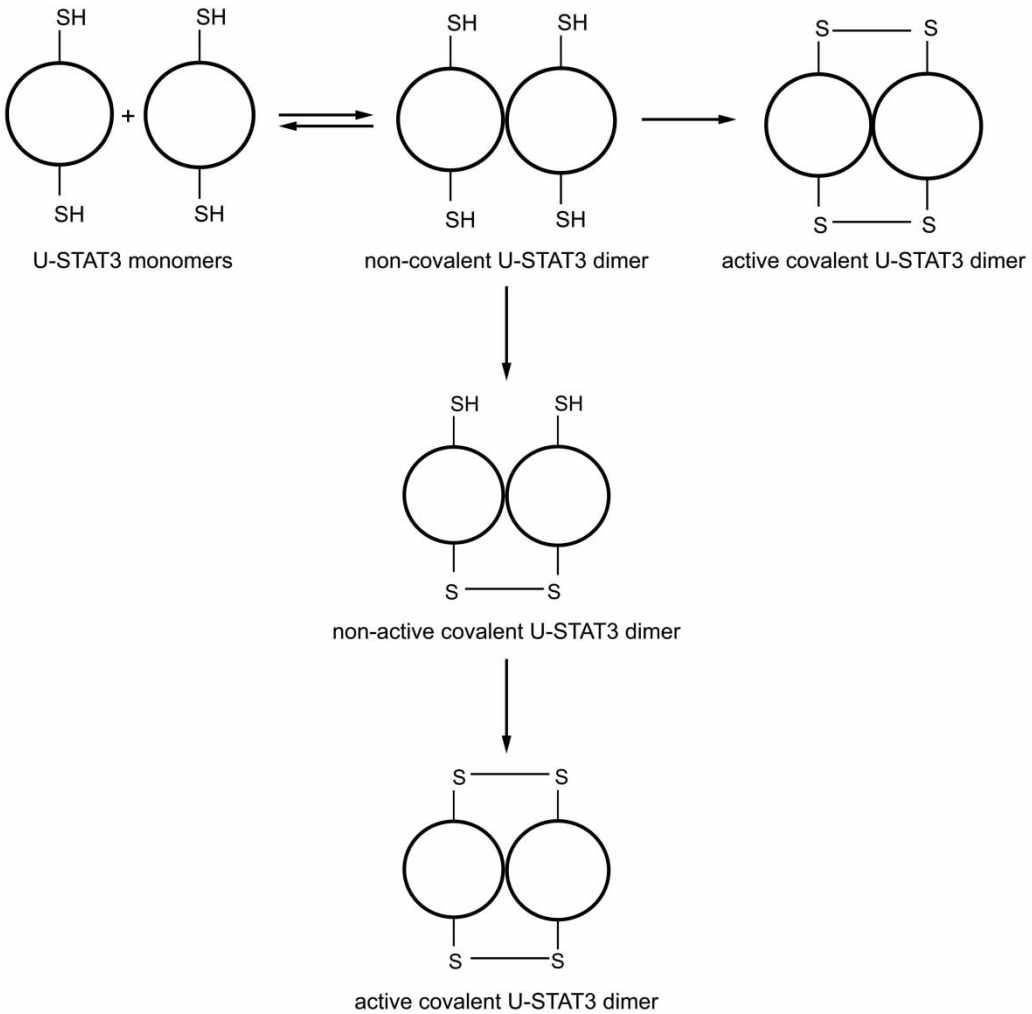

Figure 8. Schematic representation of U-STAT3 dimerization.

The three-state and four-state pathways proposed for U-STAT3 dimerization process and leading to the same active product are depicted. Our data cannot discriminate between the two proposed pathways.

Dimerization is crucial for the biological activity of U-STAT3, as only the dimeric form is able to bind DNA and to promote gene expression. In this respect, the interchain disulfide bridges play a fundamental role as they substantially contribute to the stabilization of the protein dimer. In particular, the Cys367–Cys542 disulfide bridge has been shown here to be critical for U-STAT3 DNA-binding activity. Mutation of these two Cys residues completely abolished the DNA-binding capability of U-STAT3, although the protein is still in the dimeric form, indicating that the absence of this S–S bridge might induce structural changes altering the overall conformation of the dimeric species. Recently, we reported that modification of the intracellular redox state induces inhibition of STAT3 activity through the reversible oxidation of thiol groups and identified two glutathionylated cysteine residues, Cys328 and Cys542, within the DBD and the LD, respectively [11], and further partially glutathionylated Cys367 and Cys426 (unpublished data). The involvement of the same cysteine residues in the disulfide bond-mediated U-STAT3 dimerization suggests that these S–S bridges could stabilize the dimer formation in an *in vivo* system, thus originating the correct conformation for DNA binding. Disulfide bond formation is rather a rare event within the reducing environment of cells. The recent discovery of a number of cytosolic proteins that use specific and reversible disulfide bond as a functional switch suggests that this view needs to be revised. Redox-sensitive proteins possess cysteine residues that exist as thiolate anions at neutral pH due to the lowering of their pK_a values by charge interactions with neighboring amino acid residues, and are therefore more vulnerable to oxidation [32]. In the cytoplasm, multiple pathways are involved in

the reduction of disulfide bonds that occur as part of the catalytic cycle of a variety of metabolic enzymes. Recent reports pointed out that STAT3 exists in the cytosol in complex with the disulfide isomerase ERP57 and advanced the occurrence of a sophisticated redox regulation of the protein activity. Anyway, it should be noted that some conflicting results have also been reported on STAT3/ERp57 interaction and function [25,33–36]. Thus, our findings upon U-STAT3 dimer stabilization through S–S interchain bond formation open up new scenarios on STAT3 signaling, suggesting that the chaperone ERp57 may regulate signaling by sequestering inactive and activated STAT3.

In a very recent work, Sgrignani et al. [37] used an integrated modeling approach based on protein–protein docking and molecular dynamics simulations to predict the three-dimensional architecture of U-STAT3 dimers, resulting in two distinct, noncovalent dimers with significantly different interfaces. The spatial distribution of Cys328, Cys542, Cys367, and Cys426 in the resulting computational models is not compatible with the formation of the two disulfide bonds observed in the present study. However, it should be noted that the three-dimensional structure of the two predicted U-STAT3 dimers is mutually exclusive and involves substantially different regions of the NT- and SH2-domains, thus suggesting that, at least in the first steps, the dimerization of U-STAT3 occurs by noncovalent interactions that may involve a rather plastic interface. This concept is fully in line with our results, as our spectroscopic investigations confirmed that noncovalent interactions are sufficient for proper folding and dimer formation, but that interchain disulfide bonds are needed to preserve and stabilize the functional dimer. Overall, the presented data allow us to propose a reaction scheme for U-STAT3 dimerization in a three-state process by means of two kinetic barriers or in a four-state by means of three kinetics barriers. The proposed U-STAT3 dimerization process occurs through initial rapid noncovalent interaction between U-STAT3 core fragments eventually stabilized by the formation of disulfide bonds (Figure 8).

It has been reported that STAT3 performed its function through protein–protein interactions, many of which depend on NT-domains and that NT-domain interactions are fundamental for dimer formation and stability [38,39]. Our data do not exclude the importance of initial noncovalent NT–NT domains' interaction in STAT3 dimer formation, but underline that noncovalent interactions might occur even in the recombinant protein lacking the NT-domain, suggesting that other regions of U-STAT3 may compensate for the absence of the dimerizing interactions normally contributed by the NT-domain. Thus, further studies are needed to clarify the molecular mechanism of U-STAT3 dimerization.

Abbreviations

CCD, coiled-coil domain; CD, circular dichroism spectroscopy; DBD, DNA-binding domain; DLS, dynamic light scattering; DTT, 1,4-dithiothreitol; EMSA, electrophoretic mobility shift assay; GAS, gamma-activation sequence; IκB, inhibitor of NFκB; JAK2, Janus kinase 2; LD, linker domain; NTD, N-terminal domain; pSTAT3, phosphorylated STAT3; RU, resonance units; SEC, size-exclusion chromatography; SH2, Src homology 2 domain; SPR, surface plasmon resonance; STAT3, signal transducer and activator of transcription 3; TFA, trifluoroacetic acid; TAD, transcription activation domain; U-NFκB, unphosphorylated NFκB; U-STAT3, unphosphorylated STAT3; WT, wild type.

Author Contribution

E.B. planned the research, performed and analyzed the experiments, and wrote the paper. G.G. and D.D. planned and performed some experiments and wrote the relative parts of the paper. G.C., V.M., D.C., F.C. and M.M. performed some experiments. P.P. planned and analyzed some experiments. S.M. planned the research, analyzed the experiments and wrote the paper.

Funding

This work was supported by funds from the Italian Ministry for Research and Education [FUR2012MS and FUR2013MS].

Competing Interests

The Authors declare that there are no competing interests associated with the manuscript.

References

1 Heinrich, P.C., Behrmann, I., Müller-Newen, G., Schaper, F. and Graeve, L. (1998) Interleukin-6-type cytokine signalling through the gp130/Jak/STAT pathway. *Biochem. J.* **334**, 297–314 doi:10.1042/bj3340297

Biochemical Journal (2016) **473** 3205–3219
DOI: 10.1042/BCJ20160294

2 Nagata, Y. and Todokoro, K. (1996) Interleukin 3 activates not only JAK2 and STAT5, but also Tyk2, STAT1, and STAT3. *Biochem. Biophys. Res. Commun.* **221**, 785–789 doi:10.1006/bbrc.1996.0674
3 Darnell, Jr, J.E. (1997) STATs and gene regulation. *Science* **277**, 1630–1635 doi:10.1126/science.277.5332.1630
4 Shuai, K. and Liu, B. (2003) Regulation of JAK-STAT signalling in the immune system. *Nat. Rev. Immunol.* **3**, 900–911 doi:10.1038/nri1226
5 Benekli, M., Baumann, H. and Wetzler, M. (2009) Targeting signal transducer and activator of transcription signaling pathway in leukemias. *J. Clin. Oncol.* **27**, 4422–4432 doi:10.1200/JCO.2008.21.3264
6 Hendry, L. and John, S. (2004) Regulation of STAT signalling by proteolytic processing. *Eur. J. Biochem.* **271**, 4613–4620 doi:10.1111/j.1432-1033.2004.04424.x
7 Johnston, P.A. and Grandis, J.R. (2011) STAT3 signaling: anticancer strategies and challenges. *Mol. Interv.* **11**, 18–26 doi:10.1124/mi.11.1.4
8 Kamimura, D., Ishihara, K. and Hirano, T. (2003) IL-6 signal transduction and its physiological roles: the signal orchestration model. *Rev. Physiol. Biochem. Pharmacol.* **149**, 1–38 PMID: 12687404
9 Bournazou, E. and Bromberg, J. (2013) Targeting the tumor microenvironment: JAK-STAT3 signaling. *JAKSTAT* **2**, e23828 PMID: 24058812
10 Yuan, Z.-l., Guan, Y.-j., Chatterjee, D. and Chin, Y.E. (2005) Stat3 dimerization regulated by reversible acetylation of a single lysine residue. *Science* **307**, 269–273 doi:10.1126/science.1105166
11 Butturini, E., Darra, E., Chiavegato, G., Cellini, B., Cozzolino, F., Monti, M. et al. (2014) S-Glutathionylation at Cys328 and Cys542 impairs STAT3 phosphorylation. *ACS Chem. Biol.* **9**, 1885–1893 doi:10.1021/cb500407d
12 Ulane, C.M., Rodriguez, J.J., Parisien, J.-P. and Horvath, C.M. (2003) STAT3 ubiquitylation and degradation by mumps virus suppress cytokine and oncogene signaling. *J. Virol.* **77**, 6385–6393 doi:10.1128/JVI.77.11.6385-6393.2003
13 Komyod, W., Bauer, U.-M., Heinrich, P.C., Haan, S. and Behrmann, I. (2005) Are STATS arginine-methylated? *J. Biol. Chem.* **280**, 21700–21705 doi:10.1074/jbc.C400606200
14 Kim, J., Won, J.-S., Singh, A.K., Sharma, A.K. and Singh, I. (2014) STAT3 regulation by S-nitrosylation: implication for inflammatory disease. *Antioxid. Redox Signal.* **20**, 2514–2527 doi:10.1089/ars.2013.5223
15 Danese, S. and Mantovani, A. Inflammatory bowel disease and intestinal cancer: a paradigm of the Yin–Yang interplay between inflammation and cancer. *Oncogene* **29**, 3313–3323 doi:10.1038/onc.2010.109
16 Atreya, R. and Neurath, M.F. (2008) Signaling molecules: the pathogenic role of the IL-6/STAT-3 trans signaling pathway in intestinal inflammation and in colonic cancer. *Curr. Drug Targets* **9**, 369–374 doi:10.2174/138945008784221116
17 Mariotto, S., Esposito, E., Di Paola, R., Ciampa, A., Mazzon, E., de Prati, A.C. et al. (2008) Protective effect of Arbutus unedo aqueous extract in carrageenan-induced lung inflammation in mice. *Pharmacol. Res.* **57**, 110–124 doi:10.1016/j.phrs.2007.12.005
18 Andrés, R.M., Payá, M., Montesinos, M.C., Ubeda, A., Navalón, P., Herrero, M. et al. (2013) Potential antipsoriatic effect of chondroitin sulfate through inhibition of NF-κB and STAT3 in human keratinocytes. *Pharmacol. Res.* **70**, 20–26 doi:10.1016/j.phrs.2012.12.004
19 Toffanin, S., Friedman, S.L. and Llovet, J.M. (2010) Obesity, inflammatory signaling, and hepatocellular carcinoma—an enlarging link. *Cancer Cell* **17**, 115–117 doi:10.1016/j.ccr.2010.01.018
20 Turkson, J. and Jove, R. (2000) STAT proteins: novel molecular targets for cancer drug discovery. *Oncogene* **19**, 6613–6626 doi:10.1038/sj.onc.1204086
21 Yu, H., Pardoll, D. and Jove, R. (2009) STATs in cancer inflammation and immunity: a leading role for STAT3. *Nat. Rev. Cancer* **9**, 798–809 doi:10.1038/nrc2734
22 Yang, J. and Stark, G.R. (2008) Roles of unphosphorylated STATs in signaling. *Cell Res.* **18**, 443–451 doi:10.1038/cr.2008.41
23 Yang, J., Chatterjee-Kishore, M., Staugaitis, S.M., Nguyen, H., Schlessinger, K., Levy, D.E. et al. (2005) Novel roles of unphosphorylated STAT3 in oncogenesis and transcriptional regulation. *Cancer Res.* **65**, 939–947 PMID: 15705894
24 Novak, U., Ji, H., Kanagasundaram, V., Simpson, R. and Paradiso, L. (1998) STAT3 forms stable homodimers in the presence of divalent cations prior to activation. *Biochem. Biophys. Res. Commun.* **247**, 558–563 doi:10.1006/bbrc.1998.8829
25 Ndubuisi, M.I., Guo, G.G., Fried, V.A., Etlinger, J.D. and Sehgal, P.B. (1999) Cellular physiology of STAT3: where's the cytoplasmic monomer? *J. Biol. Chem.* **274**, 25499–25509 doi:10.1074/jbc.274.36.25499
26 Yang, J., Liao, X., Agarwal, M.K., Barnes, L., Auron, P.E. and Stark, G.R. (2007) Unphosphorylated STAT3 accumulates in response to IL-6 and activates transcription by binding to NFκB. *Genes Dev.* **21**, 1396–1408 doi:10.1101/gad.1553707
27 Timofeeva, O.A., Chasovskikh, S., Lonskaya, I., Tarasova, N.I., Khavrutskii, L., Tarasov, S.G. et al. (2012) Mechanisms of unphosphorylated STAT3 transcription factor binding to DNA. *J. Biol. Chem.* **287**, 14192–14200 doi:10.1074/jbc.M111.323899
28 Duan, Z., Bradner, J., Greenberg, E., Mazitschek, R., Foster, R., Mahoney, J. et al. (2007) 8-Benzyl-4-oxo-8-azabicyclo[3.2.1]oct-2-ene-6,7-dicarboxylic acid (SD-1008), a novel Janus kinase 2 inhibitor, increases chemotherapy sensitivity in human ovarian cancer cells. *Mol. Pharmacol.* **72**, 1137–1145 doi:10.1124/mol.107.038117
29 Ma, X. and Sayeski, P.P. (2007) Identification of tubulin as a substrate of Jak2 tyrosine kinase and its role in Jak2-dependent signaling. *Biochemistry* **46**, 7153–7162 doi:10.1021/bi700101n
30 Marino, V., Astegno, A., Pedroni, M., Piccinelli, F. and Dell'Orco, D. (2014) Nanodevice-induced conformational and functional changes in a prototypical calcium sensor protein. *Nanoscale* **6**, 412–423 doi:10.1039/C3NR04978G
31 Nkansah, E., Shah, R., Collie, G.W., Parkinson, G.N., Palmer, J., Rahman, K.M. et al. (2013) Observation of unphosphorylated STAT3 core protein binding to target *ds*DNA by PEMSA and X-ray crystallography. *FEBS Lett.* **587**, 833–839 doi:10.1016/j.febslet.2013.01.065
32 Cumming, R.C., Andon, N.L., Haynes, P.A., Park, M., Fischer, W.H. and Schubert, D. (2004) Protein disulfide bond formation in the cytoplasm during oxidative stress. *J. Biol. Chem.* **279**, 21749–21758 doi:10.1074/jbc.M312267200
33 Eufemi, M., Coppari, S., Altieri, F., Grillo, C., Ferraro, A. and Turano, C. (2004) ERp57 is present in STAT3–DNA complexes. *Biochem. Biophys. Res. Commun.* **323**, 1306–1312 doi:10.1016/j.bbrc.2004.09.009
34 Chichiarelli, S., Gaucci, E., Ferraro, A., Grillo, C., Altieri, F., Cocchiola, R. et al. (2010) Role of ERp57 in the signaling and transcriptional activity of STAT3 in a melanoma cell line. *Arch. Biochem. Biophys.* **494**, 178–183 doi:10.1016/j.abb.2009.12.004
35 Guo, G.G., Patel, K., Kumar, V., Shah, M., Fried, V.A., Etlinger, J.D. et al. (2002) Association of the chaperone glucose-regulated protein 58 (GRP58/ER-60/ERp57) with Stat3 in cytosol and plasma membrane complexes. *J. Interferon Cytokine Res.* **22**, 555–563 doi:10.1089/10799900252982034

36 Sehgal, P.B., Guo, G.G., Shah, M., Kumar, V. and Patel, K. (2002) Cytokine signaling: STATS in plasma membrane rafts. *J. Biol. Chem.* **277**, 12067–12074 doi:10.1074/jbc.M200018200
37 Sgrignani, J., Olsson, S., Ekonomiuk, D., Genini, D., Krause, R., Catapano, C.V. et al. (2015) Molecular determinants for unphosphorylated STAT3 dimerization determined by integrative modeling. *Biochemistry* **54**, 5489–5501 doi:10.1021/bi501529x
38 Braunstein, J., Brutsaert, S., Olson, R. and Schindler, C. (2003) STATs dimerize in the absence of phosphorylation. *J. Biol. Chem.* **278**, 34133–34140 doi:10.1074/jbc.M304531200
39 Ren, Z., Mao, X., Mertens, C., Krishnaraj, R., Qin, J., Mandal, P.K. et al. (2008) Crystal structure of unphosphorylated STAT3 core fragment. *Biochem. Biophys. Res. Commun.* **374**, 1–5 doi:10.1016/j.bbrc.2008.04.049